ACS APPLIED MATERIALS & INTERFACES

www.acsami.org

Research Article

Cell–Cell Adhesion-Driven Contact Guidance and Its Effect on Human Mesenchymal Stem Cell Differentiation

Guillaume Le Saux,[#] Ming-Chung Wu,[#] Esti Toledo, Yin-Quan Chen, Yu-Jui Fan, Jean-Cheng Kuo,* and Mark Schvartzman*

Cite This: *ACS Appl. Mater. Interfaces* 2020, 12, 22399–22409

Read Online

ACCESS | Metrics & More | Article Recommendations | Supporting Information

ABSTRACT: Contact guidance has been extensively explored using patterned adhesion functionalities that predominantly mimic cell–matrix interactions. Whether contact guidance can also be driven by other types of interactions, such as cell–cell adhesion, still remains a question. Herein, this query is addressed by engineering a set of microstrip patterns of (i) cell–cell adhesion ligands and (ii) segregated cell–cell and cell–matrix ligands as a simple yet versatile set of platforms for the guidance of spreading, adhesion, and differentiation of mesenchymal stem cells. It was unprecedently found that micropatterns of cell–cell adhesion ligands can induce contact guidance. Surprisingly, it was found that patterns of alternating cell–matrix and cell–cell strips also induce contact guidance despite providing a spatial continuum for cell adhesion. This guidance is believed to be due to the difference between the potencies of the two adhesions. Furthermore, patterns that combine the two segregated adhesion functionalities were shown to induce more human mesenchymal stem cell osteogenic differentiation than monofunctional patterns. This work provides new insight into the functional crosstalk between cell–cell and cell–matrix adhesions and, overall, further highlights the ubiquitous impact of the biochemical anisotropy of the extracellular environment on cell function.

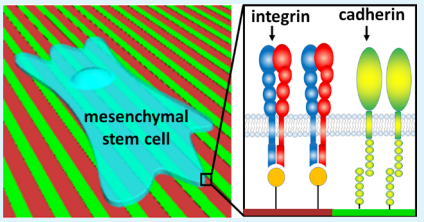

KEYWORDS: *contact guidance, cell–cell adhesion, cell–matrix adhesion, anisotropic micropatterns, stem cell differentiation*

1. INTRODUCTION

Anisotropy is a ubiquitous characteristic of the cell environment. A substantial part of this environment consists of the extracellular matrix (ECM), an intricate network of macromolecules primarily made up of fibrous and thus anisotropic proteins.[1] Variations in the composition of the ECM and in the way its components are organized give rise to a huge diversity of topographies, each adapted to the functional requirements of the particular tissue.[2] For example, tendons are composed of fibers that are organized in a hierarchical and anisotropic fashion.[3] Bones are also known to possess distinct elastic properties depending on the orientation of bone fibers.[4] There is a strong correlation between the anisotropy of the cell environment and cell function.[5] In endothelial cells, for instance, anisotropic surfaces induced a mechanical deformation of the cell nucleolus *via* cytoskeletal tension.[6] Others highlighted the importance of osteoblasts in the regulation of bone anisotropy, where the abnormal adhesion of osteoblasts resulted in the disruption of apatite alignment and the formation of spongious bone.[7] Neuron attachment, alignment, and proliferation are also stimulated on anisotropic architectures.[8] Finally, through controlled cell adhesions, anisotropic patterns differentially influenced stem cell alignment and differentiation.[9] Thus, the anisotropy of the cell environment is transduced into cell alignment and therefore influences its behavior.[10]

A prominent manifestation of extracellular anisotropy is contact guidance. the phenomenon whereby cells align and migrate along fibers. *In vitro*, contact guidance can be modeled by artificial cell environments having anisotropic topographies such as grooves and ridges[11] or chemical patterns.[12] Such chemical patterns can be based on functionalities for electrostatic interactions with cells,[13] surface-bound growth factors,[14] or the pro-adhesive RGD peptide sequence.[15] Using anisotropic surfaces to study contact guidance, it was found that geometry is transduced into biochemical signals, resulting in controlled cell functional response.[16] Examples of such a control include switching from growth to apoptosis induced by micropatterned substrates of decreasing size,[17] nucleus deformation, and gene changes in fibroblasts induced by microgrooved substrates.[18] Asymmetric patterns of alkanethiol self-assembled monolayers were also shown to effectively direct fibroblast migration[19] as well as the differentiation of stem cells.[20]

Although platforms for the study of contact guidance have been extensively explored for many years, they have so far been limited to driving the adhesion of integrins, ubiquitous receptors that link the actin cytoskeleton inside the cell and ECM proteins.[21] On the other hand, anisotropy is also present in cell

Received: November 18, 2019
Accepted: April 23, 2020
Published: April 23, 2020

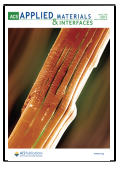

environments other than the ECM.[22] This raises the following question: is contact guidance exclusive to cell−matrix interactions, or can it be observed for other receptors that interact with cells? Specifically, can it be produced by cell−cell adhesion receptors? Addressing this question is important because intercellular forces, which are mediated by cell−cell adhesive molecules called cadherins, are also known to be critical in cell and tissue polarity[23,24] as well as the anisotropy of force distribution in cell migration.[22,25] Notably, cadherins, which form a direct link between the adjacent cell and cytoskeleton,[26] are required for the establishment of left−right asymmetry in early embryonic development.[27]

Herein, to explore the impact of anisotropy on cell−cell interactions, chemically patterned surfaces were engineered to steer cadherin-based contact guidance (see Figure 1a). The

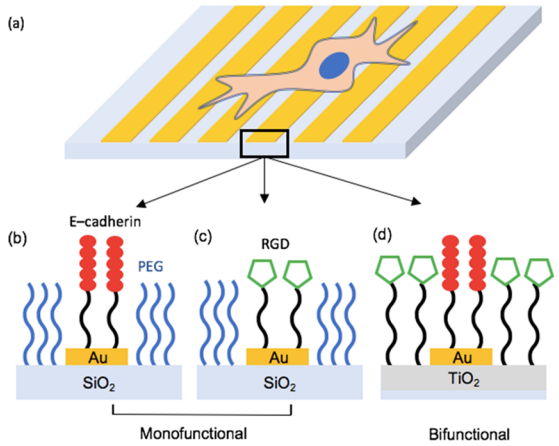

Figure 1. Biofunctional surfaces for the study of human mesenchymal stem cell (hMSC) adhesion and differentiation. (a) Schematic depiction of hMSCs adhering on biofunctionalized substrates consisting of alternating metallic strips with periods of 5−150 μm. Monofunctional substrates are composed of a SiO_2 background, which is passivated with silane-PEG to prevent nonspecific adhesion. Then, the Au strips are either (b) derivatized with Ni(II)-NTA-terminated monolayers *via* thiol chemistry, followed by attachment of histidine-tagged E-cadherin, or (c) modified with carboxyl-terminated alkyl thiols. Then, the GRGDS peptide sequence is coupled to the carboxyl moieties *via* amide linkage. (d) Bifunctional surfaces are composed of a TiO_2 background, which is modified with a carboxyl-terminated monolayer *via* phosphonic acid chemistry, followed by attachment of GRGDS through peptide linkage. Finally, gold is functionalized with Ni(II)-NTA-terminated monolayers *via* thiol chemistry, followed by attachment of histidine-tagged E-cadherin.

surfaces consisted of alternating strips of (i) gold functionalized with histidine-tagged E-cadherin *via* Ni-NTA-terminated alkyl thiols and (ii) glass functionalized with ethoxysilane poly(ethylene glycol) (silane-PEG) (Figure 1b). Here, PEG was used for its well-established antifouling properties.[28] To compare between cadherin-mediated contact guidance and integrin-mediated contact guidance, alternating strips of (i) RGD grafted onto carboxyl-terminated alkyl thiol on gold *via* peptide linkage and (ii) silane-PEG-modified glass to produce cell−ECM-mediated contact guidance were prepared (Figure 1c). Bifunctional surface patterning has been previously used to promote cell adhesion, proliferation, differentiation, and activation.[29−32] Notably, multifunctional micropatterns were recently used to modulate stem cell differentiation, focusing, however, on the effect of spatial segregation of two molecules on stem cell differentiation rather than on the anisotropy of the molecule arrangement.[33] Human mesenchymal stem cells were chosen as a case study since contact guidance was previously established for this cell type, and anisotropy is an important modulator of both cellular adhesion and osteospecific function.[34] It was demonstrated that human mesenchymal stem cells (hMSCs) could be guided to adhere to E-cadherin-functionalized microstrips and that, on sufficiently narrow lines, cells elongated in the strip direction. To the best of our knowledge, it is the first occurrence where contact guidance is observed for E-cadherin. It must be noted that cell−cell and cell−ECM adhesions are not completely separated from each other. The signaling crosstalk of integrins and cadherins has long been demonstrated[35] and is known to be crucial for directional collective cell migration and guiding tissue development.[36] This occurs despite the fact that these two molecules are spatially isolated from each other.[37] This spatial isolation is maintained throughout cell development, during which the cell environment gradually transitions from one that is rich in cell−cell interactions to one that is dominated by cell−ECM interactions. Although cadherin and integrin crosstalk is known to influence epithelial and muscle cell behavior on anisotropic surfaces,[38,39] the way cell−cell and cell−matrix cues converge to regulate MSC differentiation is still mostly unclear.[40] To model the spatial isolation between cell−cell and cell−matrix adhesions, anisotropic bifunctional surfaces were prepared to allow the selective and controlled manipulation and segregation of different cell−cell and cell−ECM ligands. These surfaces consist of alternating patterned microstrips of TiO_2 and gold, which were selectively biofunctionalized with RGD and E-cadherin *via* peptide linkage and Ni-NTA−histidine conjugations, respectively (Figure 1d). hMSC behavior was probed on bifunctional surfaces and showed that contact guidance was maintained, albeit to a lesser extent than for monofunctional surfaces. Importantly, it was demonstrated that, when spatially segregated on anisotropic surfaces, cell−cell and cell−ECM cues induce more hMSC osteogenic differentiation than on monofunctional surfaces consisting only of ligand types. Overall, this work provides a novel perspective on the interplay between integrins at focal adhesions and cadherins at adherens junctions, which lead to the spatial organization of molecular signals and forces that determine cell fate.

2. MATERIALS AND METHODS

2.1. Monofunctional Surfaces. Glass coverslips (22 × 22 mm) were photolithographically patterned to obtain strips with 5 to 150 μm widths. To ensure that, apart from periodicity, all other conditions are kept identical and to facilitate the simultaneous analysis of the cells on all the strips, the photolithography mask included areas with all strip widths. Then, 15 nm Ti and 15 nm Au were successively evaporated, resulting in 30 nm-wide strips of gold on glass after complete removal of the photoresist in acetone. The bare glass surface was passivated by a self-assembled monolayer of poly(ethylene glycol) (PEG) to prevent nonspecific binding of proteins to the surface. The PEG solution was prepared by dissolving ∼2 mg of $(PEG)_n$-Si-$(OEt)_3$ (M_w = 5000 Da, Nanocs) in 20 mL of anhydrous toluene and adding 20 μL of glacial acetic acid as a catalyst. After plasma cleaning, the samples were immersed into the PEG solution for 48 h, followed by immediate rinsing with toluene, isopropanol, ethanol, and DI water and drying under a stream of nitrogen. For RGD functionalization, gold strips were then modified with a carboxyl (COOH)-terminated PEG thiol [*O*-(2-carboxyethyl)-*O*′-(2-mercaptoethyl)heptaethylene glycol, Merck, Israel; 1 mM in ethanol, overnight, RT]. After *N*-(3-dimethylaminopropyl)-*N*′-ethylcarbodiimide hydrochloride/*N*-hydroxysuccinimide (EDC/NHS, Merck, Israel, 0.2/0.1 M, in H_2O, 1 h, RT) activation of

https://dx.doi.org/10.1021/acsami.9b20939
ACS Appl. Mater. Interfaces 2020, 12, 22399−22409

the acid moieties, GRGDS (Genecust, France) was coupled to the surface *via* amide linkage (1 mM in PBS, RT, overnight). For E-cadherin functionalization, gold strips were modified with nitrilotriacetic acid-terminated thiol monolayers, as previously mentioned. After chelation of nickel, histidine-tagged E-cadherin (Sinobiological, ENCO, Israel) was attached (2 μg/mL in PBS, 4 °C). Prior to the cell experiments, to prevent potential contamination, samples were treated with penicillin−streptomycin (P/S), transferred to a sterile laminar flow hood, and stored in sterile PBS.

2.2. Bifunctional Surfaces. Substrate preparation was based on photolithographic pattering of alternating strips of Au and TiO_2 and their orthogonal functionalization with the Arg-Gly-Asp peptide (RGD) and E-cadherin ectodomain, respectively. First, 22 × 22 mm glass coverslips were coated with Ti (15 nm) and Au (15 nm), respectively, by evaporation. Then, the surfaces were patterned by photolithography with photoresist strips of 5, 10, 50, 100, and 150 μm widths. Selective etching of the gold using KI/I_2-based Au etchant and complete removal of the remaining photoresist with acetone yielded alternating strips of Au and Ti, whose surface was oxidized by exposure to air. The TiO_2 strips were functionalized with a carboxyl-terminated alkyl phosphonic acid monolayer according the protocol described in the literature.[41] Briefly, after plasma cleaning (1 min, Harrick Plasma, USA), samples were incubated in 11-phosphoundecanoic acid (5 mM, RT, overnight) and then immediately baked for 24 h at 120 °C. Following succinimidyl activation of the acid moieties using EDC/NHS (0.2/0.1 M, in H_2O, 1 h, RT), the GRGDS peptide sequence was grafted *via* amide linkage (1 mM in PBS, RT, overnight). Gold strips were modified with a nitrilotriacetic acid (NTA)-terminated alkyl thiol monolayer (NTA terminal-SAM formation reagent, Merck, Israel). Finally, after chelation of nickel using $NiCl_2 \cdot 6H_2O$ (0.5 M, 2 h, RT), histidine-tagged E-cadherin was coupled to the gold strips (2 μg/mL in PBS, 4 °C) overnight. All substrate types were treated with P/S according to the procedure mentioned above.

2.3. Characterization of RGD-Functionalized Surfaces. Whether on titanium or gold, the linker molecules used to graft RGD do not contain nitrogen species. The detection of the nitrogen-containing RGD sequence is therefore possible using X-ray photoelectron spectroscopy (XPS). To do so, COOH-terminated surfaces were prepared and one set was activated with EDC/NHS, while the other was not. All surfaces were then incubated in a GRGDS-containing solution and analyzed by XPS. Effective grafting of GRGDS was assessed *via* the high-resolution scans of the N 1s region. XPS data were collected using an X-ray photoelectron spectrometer ESCALAB 250 ultrahigh vacuum (1×10^{-9} bar) apparatus with an Al Kα X-ray source and monochromator. The X-ray beam size was 500 μm, the survey spectra were recorded with a pass energy (PE) of 150 eV, and the high-energy resolution spectra were recorded with a PE of 20 eV. To correct for charging effects, all spectra were calibrated relative to a carbon C 1s peak positioned at 284.8 eV. The processing of the XPS results was carried out using the AVANTAGE program. Because the X-ray beam is wider than the largest strips used in this study, either Ti or Ti/Au were deposited (15 nm each) on 22 × 22 cm coverslips and the surfaces were chemically modified according to the procedure previously described.

2.4. Characterization of E-Cadherin-Modified Surfaces. Due to the presence of nitrogen in the nitrilotriacetic moiety of the surface linker (NTA) as well as in the peptide backbone of E-cadherin, using XPS to characterize E-cadherin-modified surfaces is not possible. Indirect immunofluorescence was therefore used. For this, micropatterned samples were prepared and functionalized with E-cadherin (see Section 2), For immunofluorescence, first, mouse anti-human E-cadherin (Abcam, *via* Zotal, Israel; 1:40 in PBS with 5% skim milk, overnight, 4 °C) was conjugated onto E-cadherin-terminated surfaces. Then, anti-mouse Alexa Fluor 568 (Molecular Probes, *via* rhenium, Israel; 1:40 in PBS with 5% skim milk, overnight, 4 °C) was coupled to the mouse anti-human E-cadherin. Samples were first rinsed for 24 h in PBS with 0.01% Tween-20 (Merck), then twice with neat PBS, and once with DI water and finally mounted with Dako mounting gel (Agilent). Samples were then imaged using a Nikon Ti2e epifluorescence microscope equipped with the appropriate filters.

2.5. Cell Culture. The human bone marrow-derived mesenchymal stem cells (hMSCs) were purchased from Lonza (cat. #PT-2501). Cells were cultured in a growth medium, which is DMEM (low glucose) (Thermo; cat. #10567022) supplemented with 10% FBS (Thermo; cat. #12662029) and 1% penicillin/streptomycin (Thermo; cat. #15140122). Only early passage hMSCs were used. MSCs (passage 6) were plated at ∼2000 cells/cm^2 on the functionalized surface in serum-free medium for 3 h and subsequently fixed for immunofluorescence analysis or changed to the differentiation medium. MSC differentiation was carried out as described previously.[42−44] The osteogenesis induction medium (OIM) contained a growth medium, 0.1 μM dexamethasone, 5 mM β-glycerophosphate, and 50 μM L-ascorbic-2-phosphate in a culture medium. The adipogenesis induction medium (AIM) contained a growth medium, 1 μM dexamethasone, 0.5 mM 3-isobutyl-1-methylxanthine, 10 μg/mL insulin, and 100 μM indomethacin in a culture medium. The mixed differentiation medium contained 1:1 OIM/AIM.[45,46]

2.6. Antibodies and Chemicals. The antibodies used were as follows: rabbit anti-N-cadherin (GTX127345; Genetex), mouse anti-vinculin (V4505, Sigma), mouse anti-activated integrin β1 (MAB2259Z, Millipore), Alexa Fluor 488 phalloidin (A12379, Thermo), Alexa Fluor 568-anti-mouse IgG (A11031, Thermo), Alexa Fluor 488-anti-mouse IgG (A11029, Thermo), and Alexa Fluor 568-anti-rabbit IgG (A11036, Thermo). Hoechst 33342 was purchased from AAT Bioquest.

2.7. MSC Staining. The protocol of MSC staining was carried out as described previously.[46] To double-stain alkaline phosphatase (ALP) and lipid, cells were fixed in 4% paraformaldehyde at room temperature for 10 min, rinsed in PBS, and then stained with fast BCIP/NBT (Sigma) for the activity of ALP. Subsequently, cells were rinsed in 60% isopropanol at room temperature for 2 min, stained with 30 mg/mL Oil red O (Sigma) in 60% isopropanol at room temperature for 10 min, and rinsed in PBS. Finally, cell nuclei were then stained with Hoechst 33342 in PBS for the total cell count. The cells were photographed using a Nikon Eclipse TE100. Of the total cell count, the number of cells showing purple signals scattered in the cytoplasm (ALP activity) was determined as the percentage of osteogenesis, while the number of cells with red droplets accumulated in the cytoplasm (lipids; Oil red O staining) was counted as the percentage of adipogenesis.

2.8. Immunofluorescence Analysis. MSCs were fixed with 4% paraformaldehyde in cytoskeleton buffer [10 mM MES (pH 6.1), 138 mM KCl, 3 mM $MgCl_2$, and 2 mM EGTA] at room temperature for 20 min, permeabilized with cytoskeleton buffer containing 0.5% Triton X-100 at room temperature for 5 min, and blocked with blocking solution (3% BSA/0.02% Triton-X100 in PBS) at room temperature for 60 min. Subsequently, the cells were incubated with the indicated primary antibodies in blocking solution at 4 °C for 16 h and then incubated with fluorescent dye-conjugated secondary antibody at room temperature for 1 h.

2.9. Imaging and Analysis. For the vinculin/F-actin and N-cadherin/activated integrin β1 staining, epifluorescence images were obtained using a microscope (DMRBE, Leica) coupled with a 63× NA 1.4 objective lens (Leica) and a 512B EMCCD (Andor) operated by Micro-Manager 1.4 software (Leica). For the ALP/Oil red O staining, images were taken using a microscope (Nikon Eclipse TE200) coupled with a 20× NA 0.45 objective lens (Nikon) and CCD (White) operated by TCapture (White). The adhesion area, cell orientation, adhesion orientation, and actin-bundle orientation were analyzed by in-house MATLAB (MathWorks).

2.10. Statistics. SPSS was used to confirm that the data were normal distribution and equal variances. Subsequently, Student's *t*-test was used for normal distribution of the data and large datasets. Statistical significance was set at $p < 0.05$, $p < 0.01$, and $p < 0.001$. All the graphs were illustrated and plotted with Excel software (Microsoft).

3. RESULTS AND DISCUSSION

3.1. Biofunctionalization of the Surfaces Used in This Study. A variety of strategies were used to functionalize TiO_2 and gold to produce both monofunctional and bifunctional

https://dx.doi.org/10.1021/acsami.9b20939
ACS Appl. Mater. Interfaces 2020, 12, 22399−22409

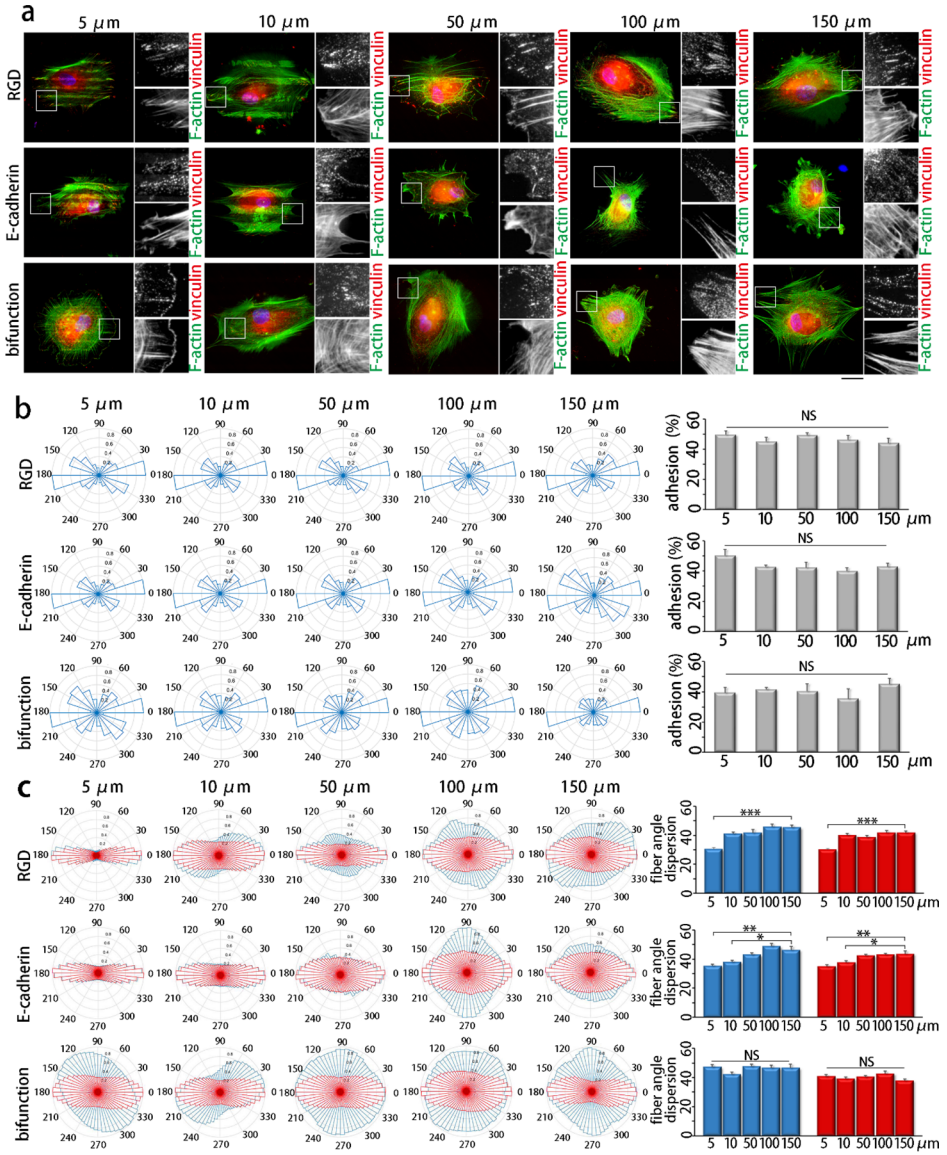

Figure 2. Impact of RGD, E-cadherin, and bifunctional microstrips on cell adhesion. Monofunctional surfaces consist of alternating Au/SiO_2 microstrips with widths ranging from 5 to 150 μm where gold is modified with RGD or E-cadherin and SiO_2 is passivated with antifouling poly(ethylene glycol). Bifunctional surfaces consist of alternating Au/TiO_2 microstrips functionalized with E-cadherin and RGD, respectively. (a) Images of immunostained vinculin (red) and phalloidin (green) in hMSCs that were mixed in serum-free medium and seeded on the surfaces for 3 h. Scale bar, 25 μm. The indicated 25 μm × 25μm boxed regions in the left image are magnified in the right two images. (b) Left: Polar histograms of the orientation of vinculin-labeled adhesions in relation to the microstrips within hMSCs plated on the surface. Right: Percentage of vinculin-labeled adhesions showing alignment with the strips (within 30°). Data are mean ± s.e.m. [RGD, n = 2741 FAs/4 cells (5 μm), 3328 FAs/4 cells (10 μm), 3656 FAs/4 cells (50 μm), 2586 FAs/4 cells (100 μm), and 3330 FAs/4 cells (150 μm); E-cadherin, n = 7638 FAs/4 cells (5 μm), 6627 FAs/4 cells (10 μm), 4506 FAs/4 cells (50 μm), 3883 FAs/4 cells (100 μm), and 4346 FAs/4 cells (150 μm); bifunction, n = 7273 FAs/4 cells (5 μm), 6498 FAs/4 cells (10 μm), 3952 FAs/4 cells (50 μm), 3820 FAs/4 cells (100 μm), and 6287 FAs/4 cells (150 μm)]. NS, not significant. (c) Left: Polar histograms of the orientation of F-actin in relation to the microstrips (blue) and the median actin-bundle orientation (red) within hMSCs plated on the surface. Right: Spread distribution of F-actin orientation in relation to the microstrips (blue) and the median actin-bundle orientation (red) was statistically calculated. Data are mean ± s.e.m. [RGD, n = 13 cells (5 μm), 12 cells (10 μm), 12 cells (50 μm), 12 cells (100 μm), and 12 cells (150 μm); E-cadherin, n = 12 cells (5 μm), 12 cells (10 μm), 11 cells (50 μm), 9 cells (100 μm), and 7 cells (150 μm); bifunction, n = 15 cells (5 μm), 11 cells (10 μm), 11 cells (50 μm), 11 cells (100 μm), and 13 cells (150 μm)]. *p < 0.05, **p < 0.01, ***p < 0.001. NS, not significant.

surfaces, which were previously described and characterized.[41,47−49] Briefly, the covalent grafting of RGD onto carboxyl-terminated TiO_2 and Au surfaces *via* peptide linkage was confirmed using XPS. The chelation of histidine-tagged E-cadherin onto Ni-NTA-modified gold strips was demonstrated using indirect immunofluorescence with an E-cadherin-specific primary antibody followed by a fluorescently labeled secondary antibody. Finally, the site-specific attachment of biomolecules onto bifunctional surfaces consisting of alternating strips of TiO_2 and Au was confirmed using indirect immunofluorescence. As a proof of principle, instead of RGD, biotin was attached to the carboxyl-functionalized TiO_2 *via* peptide linkage followed by attachment of green fluorescent NeutrAvidin. Gold was modified with histidine-tagged E-cadherin and a red fluorescent probe, as previously mentioned. Details of the characterizations

https://dx.doi.org/10.1021/acsami.9b20939
ACS Appl. Mater. Interfaces 2020, 12, 22399−22409

of the mono- and bifunctional surfaces used in this study are shown in Figures S1 and S2 (Supporting Information).

3.2. Anisotropy of Cadherin and Cadherin−RGD Pattern Induces Contact Guidance. Having demonstrated the biofunctionalization strategy, the impact of the functionalized surfaces on hMSC adhesion and orientation was investigated. To avoid cell adhesion induced by serum fibronectin[50] or cell−cell contacts by the confluent cell layer, hMSCs were suspended in serum-free medium, and cells were seeded in low density (~2000 cells/cm^2) on strips of E-cadherin and alternating RGD/E-cadherin strips for 3 h. RGD strips were also used for control as integrin-mediated contact guidance has been broadly demonstrated before.[51] After incubation, cells were stained for vinculin and phalloidin to visualize integrin-mediated[52] and cadherin-mediated[53,54] adhesions and F-actin, respectively. Vinculin is a focal adhesion marker that interacts with actin and is therefore a compelling indicator of integrin-mediated cell morphological changes.[52] Additionally, vinculin is a key component of adherens junctions mediated by E-cadherin[53] or N-cadherin,[54] thus making it an ideal means of assessment of the impact of the substrates.

Representative images of cells on RGD or E-cadherin monofunctional and alternating RGD/E-cadherin bifunctional surfaces are shown in Figure 2a. For RGD or E-cadherin monofunctional substrates, regardless of strip width, preferential cell attachment to the functionalized gold strips was observed (Figure S3, Supporting Information). Although hMSCs predominantly express N-cadherin,[55] the enhanced expression of E-cadherin on oriented E-cadherin substrates has been reported previously,[56] indicating that the homophilic E-cadherin-mediated adhesion supports cell attachment on E-cadherin monofunctional substrates. Surprisingly, N-cadherin-based adhesions, but not integrin-mediated adhesions, were detected in hMSCs when cultured on oriented E-cadherin substrates (Figure S4, Supporting Information), revealing the possibility of heterophilic binding between N-cadherin and E-cadherin. Steering cell attachment, which has been previously reported,[57] stems from the combination of pro-adhesive molecules on gold and antifouling PEG molecules and thus confirms the efficacy of passivation of glass with PEG. Conversely, on bifunctional micropatterned surfaces with widths larger than 100 μm, cells showed no pronounced attachment toward either of the biomolecules present (Figure S3, Supporting Information). This observation can be explained by the fact that alternating RGD and E-cadherin domains provide a continuous array of available anchor points for the cells.

With the confirmation that hMSCs interact specifically with the E-cadherin or RGD strips on monofunctional substrates, focus was given on how the cadherin-based cell adhesions and focal adhesions aligned with these bioactive strips (Figure 2b). Here, a value of 0° corresponds to an alignment of the vinculin-marked adhesions with the strips. About 40−50% of vinculin-marked adhesions with pronounced alignment with the strips (within 30°) were observed, regardless of the width, on E-cadherin monofunctional, RGD monofunctional, or bifunctional micropatterned surfaces (Figure 2b). These revealed that the E-cadherin and RGD peptides presented on the strips were able to guide hMSCs to adhere and assemble adhesions. Because the adhesions are dynamic structures, which coordinate with the overlying actin cytoskeleton, the organization of actin bundles was investigated. To calculate the orientation of actin bundles within a cell, the images of phalloidin-stained cells were analyzed by rotating each cell image so that the median actin-bundle orientation became horizontal. The spread of the distribution of actin-bundle orientations provides a measure of the degree of actin-bundle polarization. On RGD monofunctional or E-cadherin monofunctional surfaces, hMSCs possessed higher degrees of aligned actin-bundle orientation on narrow strips (5−10 μm) (Figure 2c, red). With increasing width of strips of RGD or E-cadherin monofunctional surfaces and bifunctional surfaces, wider distributions of actin-bundle orientation were observed (Figure 2c, red). When a criterion was set to calculate the orientation of actin bundles with respect to the direction of these bioactive strips (Figure 2c, blue), a pronounced alignment of the actin bundles with the strips was observed up to 10 μm widths on RGD or E-cadherin monofunctional surfaces (Figure 2c, blue). The wider strips (50−150 μm) of RGD or E-cadherin monofunctional surfaces and bifunctional surfaces are large enough to accommodate an entire cell; hence, no preferential directionality was noted (Figure 2c, blue). In turn, actin-bundle alignment correlates well with cell alignment (Figure S5). This phenomenon called contact guidance[12] has been previously described *in vivo*[58] as well as *in vitro* on different anisotropic substrates and for numerous cell types,[59] including mesenchymal stem cells.[20]

For the surfaces used in this study, the adhesive molecules were immobilized on metallic strips with a thickness of 30 nm. It was reported that grooves with depths as shallow as 35 nm could induce contact guidance.[60] However, in the latter work, pronounced contact guidance was maintained for grooves with a pitch-to-depth ratio of 6 and below but was gradually reduced for increasing pitch-to-depth ratios and completely vanished for micrometer-scale grooves with a pitch-to-depth ratio of ~16 and above. In the present systems, this pitch-to-depth ratio is greater than 160:1. It is therefore envisaged that topographic effects are negligible in this case. This is also supported by the fact that, in the case of MSCs, a critical width of 10 μm was necessary to guide cellular adhesion and modulate subsequent cellular functions except for 330 nm-deep grooves, which are an order of magnitude deeper than the ones in the present work.[34] Although purely chemically driven contact guidance is less explicitly reported,[13,14,61] contact guidance of MSCs was observed on 10 μm-wide strips of patterned fibronectin on an adhesion-resistant background.[62] In the present work, the fabricated patterned surfaces can be likened to ridges of gold functionalized with RGD and grooves of PEG-modified glass with a depth of 30 nm but where the depth-to-pitch ratio is too high for topography to have a notable impact. Analogous to the work on patterned fibronectin, the surfaces can guide spatial positioning of hMSCs, where adhesion is hindered by the chemical barrier stemming from the antifouling PEG moieties, while it is facilitated by the presence of RGD on the gold ridges. It is generally agreed that cell polarization is driven by the alignment of adhesion proteins to the topographic and/or chemical cues of the surface.[63] This explains why, in the present case, contact guidance is observed on the 5−10 μm-wide strips since focal adhesions have a typical length of 1−5 μm.[64] However, for the 50 μm-wide strips, it appears that it is the confinement of the entire cells, provided by PEG on glass, that drives their alignment to the micropatterns and the subsequent alignment of focal adhesions and actin bundles, although the functionalized surface did not influence the anisotropic orientation of actin bundles of hMSCs.

As previously mentioned, it was found that both adhesion actin-bundle linkages and cell alignment occurred on E-

https://dx.doi.org/10.1021/acsami.9b20939
ACS Appl. Mater. Interfaces 2020, 12, 22399−22409

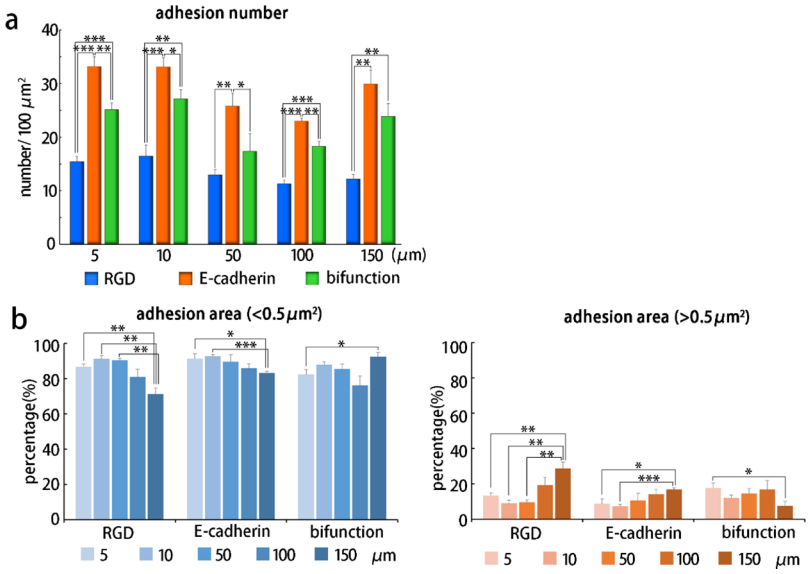

Figure 3. Impact of RGD, E-cadherin, and bifunctional microstrips on cell adhesion formation and maturation. hMSCs in serum-free medium were plated on the microstrips for 3 h, and then images were captured by epifluorescence microscopy, as shown in Figure 2a. (a) The plot shows the number of segmented vinculin-marked adhesions per 100 μm^2 cell spreading area. (b) These plots show the percentage of vinculin-marked adhesions with area under 0.5 μm^2 (left) and above 0.5 μm^2 (right) within a single cell. In (a) and (b), data are mean ± s.e.m. [RGD, n = 2741 FAs/4 cells (5 μm), 3328 FAs/4 cells (10 μm), 3656 FAs/4 cells (50 μm), 2586 FAs/4 cells (100 μm), and 3330 FAs/4 cells (150 μm); E-cadherin, n = 7638 FAs/4 cells (5 μm), 6627 FAs/4 cells (10 μm), 4506 FAs/4 cells (50 μm), 3883 FAs/4 cells (100 μm), and 4346 FAs/ 4 cells (150 μm); bifunction, n = 7273 FAs/ 4 cells (5 μm), 6498 FAs/4 cells (10 μm), 3952 FAs/4 cells (50 μm), 3820 FAs/4 cells (100 μm), and 6287 FAs/4 cells (150 μm)]. *p < 0.05, **p < 0.01, ***p < 0.001.

cadherin-modified strips with widths of 5 and 10 μm but markedly less for widths of 50 μm and above (Figure 2b,c and Figure S5, Supporting Information). Cadherins were previously used to promote cell adhesion *via* adherens junctions[65] and for stem cells in particular.[54,56] Still, this is the first time that cadherin-induced contact guidance is observed. Cadherin strips were previously used to control the migration of cells, but these patterns did not induce any observable contact guidance, presumably because of the absence of any antifouling agent between the cadherin strips.[38] This highlights the importance of anti-adhesive agents, such as PEG, for contact guidance. Similar to RGD micropatterns, for 5 and 10 μm-wide strips, cell alignment on cadherin-modified strips is driven by the alignment of adherens junctions.[66] However, in contrast to RGD, contact guidance visibly wanes on 50 μm-wide strips and therefore suggests that, although PEG passivation prevents cell spreading onto the glass strips, E-cadherin-mediated adhesion may not be strong enough to steer cell alignment to the extent that RGD does.

Even more surprisingly, guidance of the vinculin-mediated adhesions was observed on RGD/E-cadherin bifunctional microstrips with widths equal to or smaller than the cell size, i.e., 5 and 10 μm. Similar to vinculin-mediated adhesions, cells aligned along the 5 μm-wide microstrips (Figure S5, Supporting Information). This result is intriguing. On the one hand, bifunctional surfaces provide a continuous layer of pro-adhesive molecules. On the other hand, it is obvious that cells can still sense the geometry of the spatial segregation between these two types of molecules. As suggested previously, the contact guidance analysis of monofunctional RGD and E-cadherin strips reveals that, although both surface types induce contact guidance—the one observed on RGD is more pronounced since it can be observed on microstrips up to 50 μm wide, which is not the case for E-cadherin. This is an indication that there are two effects that may be simultaneously at play to explain such a behavior. First, using the very same surface chemistry, the surface density of biomolecules immobilized onto TiO_2 was found to be higher than that onto Au, with values of 130 and 30 fmol/mm^2 for TiO_2 and Au, respectively.[41] In both cases, the surface density is higher than the reported threshold of 1 fmol/mm^2 of cell adhesion molecules sufficient to promote adhesion and spreading for both integrin-mediated[67] and cadherin-mediated adhesions.[68] Remarkably, this threshold was established based on arrays of segregated ligands separated by tens of nanometers, whereas continuous layers were used in the present case, and these continuous layers provide the maximal surface density of both ligands to the cells. Importantly, this also implies that the differences in surface densities, if they exist, cannot explain alone the contact guidance on bifunctional surfaces. In contrast, second, it was found that the force per E-cadherin-mediated adhesion is 3.6 nN/μm^2,[69] while that of integrin-mediated adhesion is 5.5 nN/μm^2.[70] While these values are close, their conjunction with the differences in surface densities between TiO_2 and Au reveals that the overall adhesion strength on RGD-modified TiO_2 is ∼6 times greater than that on E-cadherin-modified Au. This combination between the differences in surface densities and adhesion strengths creates a contrast between cadherin- and integrin-mediated adhesions, and it is plausible that this contrast is the driving force behind the observed contact guidance on the alternating RGD−E-cadherin strips.

3.3. Stem Cell Osteogenic Commitment Correlates with Contact Guidance and Adhesion Signals. With the confirmation that hMSCs were able to form aligned adhesions on the RGD- or E-cadherin-presenting strips of our substrates, whether these bioactive strips regulated adhesion formation and maturation was further investigated. It was found that, within the same width of the strip, hMSCs on the E-cadherin monofunc-

https://dx.doi.org/10.1021/acsami.9b20939
ACS Appl. Mater. Interfaces 2020, 12, 22399−22409

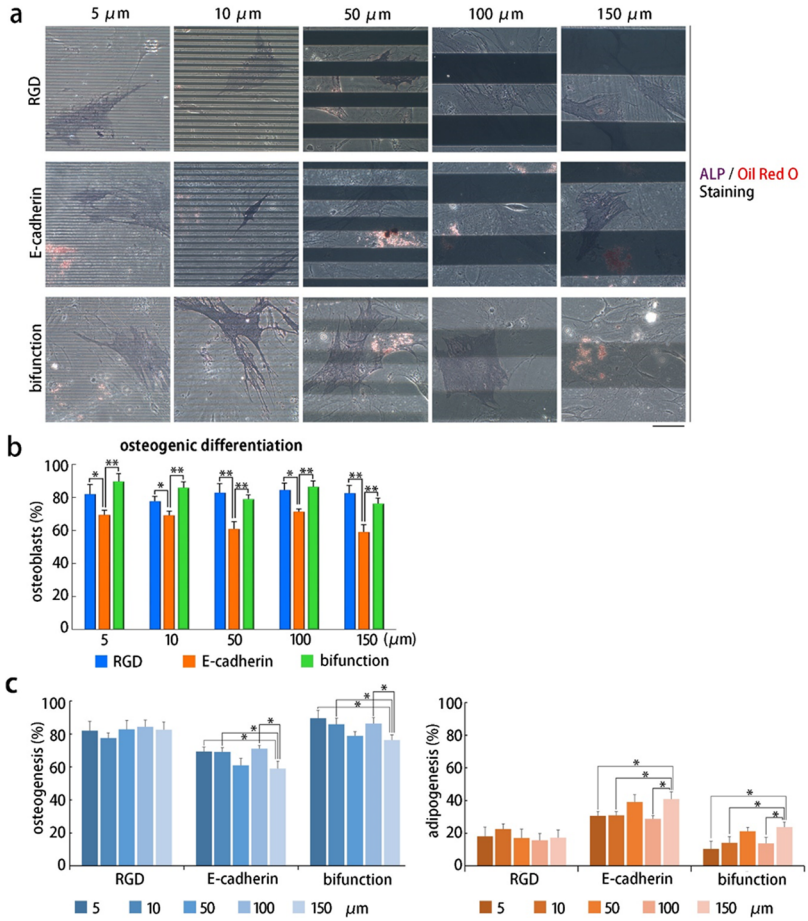

Figure 4. Impact of RGD, E-cadherin, and bifunctional microstrips on hMSC differentiation. (a) Images of hMSCs in serum-free medium plated on RGD monofunctional, E-cadherin monofunctional, and bifunctional surfaces for 3 h and then switched to a mixed differentiation medium [osteogenesis induction medium (OIM)/adipogenesis induction medium (AIM) = 1:1] for 14 days; these were stained for the presence of lipid (Oil red O; red) and ALP activity (purple). Scale bar, 100 μm. (b, c) Percentage of cells showing osteogenesis (ALP-positive cells) and adipogenesis (Oil red O-positive cells). Data are mean ± s.e.m. (n = 5 independent experiments). *$p < 0.05$, **$p < 0.01$.

tional surfaces and bifunctional micropatterned surfaces were able to form more vinculin-marked adhesions than on the RGD monofunctional surfaces (Figure 3a). These revealed the dominant effect of E-cadherin signals in adhesion formation and further supporting RGD signals for adhesion formation on bifunctional micropatterned surfaces. The size distribution of vinculin-marked adhesions was quantified, and it was found that, compared with the wider strips (150 μm), cells on the RGD (5 to 50 μm) or E-cadherin monofunctional surfaces (5 to 10 μm) contained a larger number of small adhesions (<0.5 μm^2) and a reduced number of big adhesions (>0.5 μm^2) (Figure 3b). Thus, narrow strips constrain not only the maturation process of focal adhesions but also that of E-cadherin-mediated adhesions. This supports earlier studies showing that focal adhesion maturation is physically limited by the anisotropy in strips of collagen.[71] However, on the bifunctional surfaces, a higher percentage of big adhesions (>0.5 μm^2) in hMSCs on the 5 μm-wide strips was detected when compared to the 150 μm-wide strips. Therefore, the spatially segregated signals of E-cadherin-based cell−cell adhesions and focal adhesions in a single cell can significantly activate hMSCs to promote adhesion formation and maturation process (Figure 3); this occurs most likely *via* adhesive crosstalk between E-cadherin- and integrin-mediated signals.[55,56]

Next, the effect of adhesive signals on hMSC commitment switch between osteogenic fate and adipogenic fate was explored. hMSCs plated on the strips were exposed for 14 days to a 1:1 combination of adipogenesis- and osteogenesis-promoting solution cues *via* a mixed differentiation medium [osteogenesis induction medium (OIM) and adipogenesis induction medium (AIM) in a ratio of 1:1]. In the mixed differentiation medium, hMSCs received soluble factors and were able to differentiate between osteogenic fate and adipogenic fate.[42,46] Thus, hMSCs cultured in the mixed differentiation medium can verify whether the adhesive signals on the functionalized surfaces can act specifically on the lineage commitment process. After 14 days, cells were then stained for alkaline phosphate (ALP) activity and with Oil red O for the presence of lipid droplets, which are markers of osteogenesis[72] and adipogenesis,[73] respectively (Figure 4a). Figure S6 (Supporting Information) reveals that the potential cross-reaction in the differentiation media or staining process can be excluded; thus, the percentage of hMSCs expressing ALP activity or lipid droplets for single cells was further determined, demonstrating a marked effect of adhesive signals on commitment. It was found that, regardless of the width of the strips, more cells showed ALP activity on RGD monofunctional surfaces and bifunctional surfaces and less ALP activity on E-cadherin monofunctional surfaces (Figure 4b). This result revealed the dominant effect of integrin signaling on hMSC osteogenesis. The ratio of osteogenesis to adipogenesis was

https://dx.doi.org/10.1021/acsami.9b20939
ACS Appl. Mater. Interfaces 2020, 12, 22399−22409

analyzed, and it was found that cells on the 5 μm E-cadherin monofunctional surfaces showed about 69% (69.33 ± 0.03%) osteogenesis and about 31% (30.67 ± 0.03%) adipogenesis, while cells on the wider strips (150 μm) displayed about 59% (59.05 ± 0.04%) osteogenesis and about 41% (40.95 ± 0.04%) adipogenesis. However, the width of the RGD strips did not influence the differentiation lineage of osteogenesis and adipogenesis. Interestingly, compared with the wider strips (150 μm) on the bifunctional surfaces (osteogenesis: 76.34 ± 0.03%; adipogenesis: 23.66 ± 0.03%), the narrow strips (5 μm) resulted in about 90% (89.64 ± 0.05%) osteogenesis and about 10% (10.35 ± 0.05%) adipogenesis (Figure 4b). Although RGD signaling plays a dominant role in directing hMSC osteogenesis, cells on the 5 μm-wide bifunctional strips significantly increased osteogenesis to about 90%. These results revealed that the spatially segregated adhesive signals with contact guidance were able to provide the best conditions to promote hMSC osteogenesis.

Previous studies have also used patterned substrates to study how cell−cell contacts and focal adhesions affect hMSC osteogenic commitment. These have revealed that hMSC osteogenic differentiation is restricted by signals of cadherin-mediated cell−cell adhesions and promoted by integrin-mediated signals by enhancing cytoskeletal tension.[40,46,74] These support our results that RGD monofunctional surfaces enhance hMSCs' commitment toward an osteoblast lineage, while E-cadherin monofunctional surfaces weaken osteogenic differentiation (Figure 4b). However, mixed surfaces coated with a mix of HAVDI and RGD reveal that HAVDI ligation alters ECM mechanosensing and significantly suppresses YAP/TAZ nuclear translocation to induce a soft phenotype,[40] which is predicted to suppress hMSC osteogenesis. This implies the importance of spatial segregation of E-cadherin- and integrin-mediated adhesive ligands in fate commitment of hMSCs. In our study, the bifunctional surfaces and RGD monofunctional surfaces significantly induced osteogenic differentiation, as evidenced by the higher ALP activity (Figure 4b). Interestingly, the narrower strips on the E-cadherin monofunctional surfaces increase the degree of osteogenic differentiation. This suggests that E-cadherin ligation acts as a signaling offset while giving hMSCs the ability to eventually sense contact guidance. Moreover, cells on the bifunctional surfaces presenting E-cadherin and RGD display increased osteogenic differentiation, which is more pronounced on the narrower strips (Figure 4c). Thus, spatially segregated E-cadherin-mediated cell−cell adhesion signals can alter hMSC perception of the anisotropy of the substrate and further cooperate with the integrin-mediated adhesive signals for hMSC differentiation lineage toward osteogenesis.

4. CONCLUSIONS

The influence of anisotropy in organisms is multifactorial. Contact guidance, one of the most visible manifestations of anisotropy, is known to be driven by a balance of cell−ECM and cell−cell interactions. Herein, surfaces consisting of alternating strips of chemically modified metals were designed whereby the influence of cell−ECM and cell−cell interactions could be individually assessed. Using human mesenchymal stem cells as a case study, it was unambiguously shown that surface chemistry consisting of alternating strips of pro- and anti-adhesive molecules was just as powerful as topography in inducing contact guidance. This aspect is often overlooked *in vitro* and has direct repercussions *in vivo* since the ECM contains both pro- and anti-adhesive proteins.[75] Importantly, this is the first time that contact guidance induced by cadherins was observed. It was also shown that, in the case of spatially segregated adhesive molecules known to operate in distinct pathways, not only the balance but also the contrast in adhesive forces can generate contact guidance. Finally, it was shown that spatially segregated cell−ECM and cell−cell adhesions in a single cell could significantly activate hMSCs to promote adhesion and, crucially, provided the optimal conditions to promote hMSC osteogenesis. Using a simple yet controlled system, it was demonstrated that combining anisotropy and spatially segregated multifunctionality was essential in determining cell behavior, and such a system is envisaged to be used in a wide range of applications.

■ ASSOCIATED CONTENT

Supporting Information

The Supporting Information is available free of charge at https://pubs.acs.org/doi/10.1021/acsami.9b20939.

Complementary characterizations by XPS and fluorescence microscopy, quantification of relative cell attachment, evaluation of heterophilic binding between membrane- and surface-bound cadherin and cell alignment on the mono- and bifunctional surfaces, and analysis of osteogenesis and adipogenesis induction media-induced hMSC differentiation (PDF)

■ AUTHOR INFORMATION

Corresponding Authors

Jean-Cheng Kuo − *Institute of Biochemistry and Molecular Biology and Cancer Progression Research Center, National Yang-Ming University, Taipei 11221, Taiwan;* orcid.org/0000-0003-3682-0783; Email: jckuo@ym.edu.tw

Mark Schvartzman − *Department of Materials Engineering and Isle Katz Institute for Nanoscale Science and Technology, Ben-Gurion University of the Negev, Beer-Sheva 8410501, Israel;* orcid.org/0000-0002-5912-525X; Email: marksc@bgu.ac.il

Authors

Guillaume Le Saux − *Department of Materials Engineering and Isle Katz Institute for Nanoscale Science and Technology, Ben-Gurion University of the Negev, Beer-Sheva 8410501, Israel;* orcid.org/0000-0003-4902-1980

Ming-Chung Wu − *Institute of Biochemistry and Molecular Biology, National Yang-Ming University, Taipei 11221, Taiwan*

Esti Toledo − *Department of Materials Engineering and Isle Katz Institute for Nanoscale Science and Technology, Ben-Gurion University of the Negev, Beer-Sheva 8410501, Israel*

Yin-Quan Chen − *Cancer Progression Research Center, National Yang-Ming University, Taipei 11221, Taiwan*

Yu-Jui Fan − *School of Biomedical Engineering, Taipei Medical University, Taipei 110, Taiwan;* orcid.org/0000-0003-4900-1840

Complete contact information is available at: https://pubs.acs.org/10.1021/acsami.9b20939

Author Contributions

#G.L.S. and M.-C.W. contributed equally to this work.

Notes

The authors declare no competing financial interest.

https://dx.doi.org/10.1021/acsami.9b20939
ACS Appl. Mater. Interfaces 2020, 12, 22399−22409

■ ACKNOWLEDGMENTS

This research was supported by Israel Ministry of Science and Technology and Taiwan Ministry of Science and Technology: Israel-Taiwan Collaborative Grant #3-12409. J.-C.K. is supported by research grants from the Taiwan Ministry of Science and Technology (MOST 104-2923-B-010-002-MY2, 107-2633-B-010-001, and MOST 107-2320-B-010-049), the Novel Bioengineering and Technological Approaches to Solve Two Major Health Problems in Taiwan sponsored by the Taiwan Ministry of Science and Technology Academic Excellence Program (MOST 108-2633-B-009-001), Cancer Progression Research Center (National Yang-Ming University) from The Featured Areas Research Center Program within the framework of the Higher Education Sprout Project by the Ministry of Education (MOE) in Taiwan, the Yen Tjing Ling Medical Foundation, and the Ministry of Education's "Aim for the Top University Plan".

■ REFERENCES

(1) Dyson, R. J.; Green, J. E. F.; Whiteley, J. P.; Byrne, H. M. An Investigation of the Influence of Extracellular Matrix Anisotropy and Cell−Matrix Interactions on Tissue Architecture. *J. Math. Biol.* **2016**, *72*, 1775−1809.

(2) Reddi, A. H.; Gay, R.; Gay, S.; Miller, E. J. Transitions in Collagen Types during Matrix-Induced Cartilage, Bone, and Bone Marrow Formation. *Proc. Natl. Acad. Sci. U. S. A.* **1977**, *74*, 5589−5592.

(3) Domingues, R. M. A.; Chiera, S.; Gershovich, P.; Motta, A.; Reis, R. L.; Gomes, M. E. Enhancing the Biomechanical Performance of Anisotropic Nanofibrous Scaffolds in Tendon Tissue Engineering: Reinforcement with Cellulose Nanocrystals. *Adv. Healthcare Mater.* **2016**, *5*, 1364−1375.

(4) Katz, J. L.; Meunier, A. The Elastic Anisotropy of Bone. *J. Biomech.* **1987**, *20*, 1063−1070.

(5) Thery, M.; Racine, V.; Piel, M.; Pepin, A.; Dimitrov, A.; Chen, Y.; Sibarita, J.-B.; Bornens, M. Anisotropy of Cell Adhesive Microenvironment Governs Cell Internal Organization and Orientation of Polarity. *Proc. Natl. Acad. Sci. U. S. A.* **2006**, *103*, 19771−19776.

(6) Hu, S.; Eberhard, L.; Chen, J.; Love, J. C.; Butler, J. P.; Fredberg, J. J.; Whitesides, G. M.; Wang, N. Mechanical Anisotropy of Adherent Cells Probed by a Three-Dimensional Magnetic Twisting Device. *Am. J. Physiol. Cell Physiol.* **2004**, *287*, C1184−C1191.

(7) Sekita, A.; Matsugaki, A.; Nakano, T. Disruption of Collagen/Apatite Alignment Impairs Bone Mechanical Function in Osteoblastic Metastasis Induced by Prostate Cancer. *Bone* **2017**, *97*, 83−93.

(8) Golafshan, N.; Kharaziha, M.; Fathi, M.; Larson, B. L.; Giatsidis, G.; Masoumi, N. Anisotropic Architecture and Electrical Stimulation Enhance Neuron Cell Behaviour on a Tough Graphene Embedded PVA: Alginate Fibrous Scaffold. *RSC Adv.* **2018**, *8*, 6381−6389.

(9) Peng, R.; Yao, X.; Ding, J. Effect of Cell Anisotropy on Differentiation of Stem Cells on Micropatterned Surfaces through the Controlled Single Cell Adhesion. *Biomaterials* **2011**, *32*, 8048−8057.

(10) Ballester-Beltran, J.; Biggs, M. J. P.; Dalby, M. J.; Salmeron-Sanchez, M.; Leal-Egaña, A. Sensing the Difference: The Influence of Anisotropic Cues on Cell Behavior. *Front. Mater.* **2015**, *2*, 39.

(11) Teixeira, A. I.; Abrams, G. A.; Bertics, P. J.; Murphy, C. J.; Nealey, P. F. Epithelial Contact Guidance on Well-Defined Micro- and Nanostructured Substrates. *J. Cell Sci.* **2003**, *116*, 1881−1892.

(12) Flemming, R. G.; Murphy, C. J.; Abrams, G. A.; Goodman, S. L.; Nealey, P. F. Effects of Synthetic Micro- and Nano-Structured Surfaces on Cell Behavior. *Biomaterials* **1999**, *20*, 573−588.

(13) Healy, K. E.; Lom, B.; Hockberger, P. E. Spatial Distribution of Mammalian Cells Dictated by Material Surface Chemistry. *Biotechnol. Bioeng.* **1994**, *43*, 792−800.

(14) Hauff, K.; Zambarda, C.; Dietrich, M.; Halbig, M.; Grab, A. L.; Medda, R.; Cavalcanti-Adam, E. A. Matrix-Immobilized BMP-2 on Microcontact Printed Fibronectin as an in Vitro Tool to Study BMP-Mediated Signaling and Cell Migration. *Front. Bioeng. Biotechnol.* **2015**, *3*, 62.

(15) Chollet, C.; Lazare, S.; Guillemot, F.; Durrieu, M. C. Impact of RGD Micro-Patterns on Cell Adhesion. *Colloids Surf., B* **2010**, *75*, 107−114.

(16) Vogel, V.; Sheetz, M. Local Force and Geometry Sensing Regulate Cell Functions. *Nat. Rev. Mol. Cell Biol.* **2006**, 265−275.

(17) Chen, C. S.; Mrksich, M.; Huang, S.; Whitesides, G. M.; Ingber, D. E. Geometric Control of Cell Life and Death. *Science* **1997**, *276*, 1425−1428.

(18) Dalby, M. J.; Riehle, M. O.; Yarwood, S. J.; Wilkinson, C. D. W.; Curtis, A. S. G. Nucleus Alignment and Cell Signaling in Fibroblasts: Response to a Micro-Grooved Topography. *Exp. Cell Res.* **2003**, *284*, 272−280.

(19) Jiang, X.; Bruzewicz, D. A.; Wong, A. P.; Piel, M.; Whitesides, G. M. Directing Cell Migration with Asymmetric Micropatterns. *Proc. Natl. Acad. Sci. U. S. A.* **2005**, *102*, 975−978.

(20) Kurpinski, K.; Chu, J.; Hashi, C.; Li, S. Anisotropic Mechanosensing by Mesenchymal Stem Cells. *Proc. Natl. Acad. Sci. U. S. A.* **2006**, *103*, 16095−16100.

(21) Ruoslahti, E.; Pierschbacher, M. D. New Perspectives in Cell Adhesion: RGD and Integrins. *Science* **1987**, *238*, 491−497.

(22) Matsuzawa, K.; Himoto, T.; Mochizuki, Y.; Ikenouchi, J. α-Catenin Controls the Anisotropy of Force Distribution at Cell-Cell Junctions during Collective Cell Migration. *Cell Rep.* **2018**, *23*, 3447−3456.

(23) Dupin, I.; Camand, E.; Etienne-Manneville, S. Classical Cadherins Control Nucleus and Centrosome Position and Cell Polarity. *J. Cell Biol.* **2009**, *185*, 779−786.

(24) Rübsam, M.; Mertz, A. F.; Kubo, A.; Marg, S.; Jüngst, C.; Goranci-Buzhala, G.; Schauss, A. C.; Horsley, V.; Dufresne, E. R.; Moser, M.; Ziegler, W.; Amagai, M.; Wickström, S. A.; Niessen, C. M. E-Cadherin Integrates Mechanotransduction and EGFR Signaling to Control Junctional Tissue Polarization and Tight Junction Positioning. *Nat. Commun.* **2017**, *8*, 1250.

(25) Plutoni, C.; Bazellieres, E.; Le Borgne-Rochet, M.; Comunale, F.; Brugues, A.; Séveno, M.; Planchon, D.; Thuault, S.; Morin, N.; Bodin, S.; Trepat, X.; Gauthier-Rouvière, C. P-Cadherin Promotes Collective Cell Migration via a Cdc42-Mediated Increase in Mechanical Forces. *J. Cell Biol.* **2016**, *212*, 199−217.

(26) Gumbiner, B. M. Regulation of Cadherin-Mediated Adhesion in Morphogenesis. *Nat. Rev. Mol. Cell Biol.* **2005**, *6*, 622−634.

(27) García-Castro, M. I.; Vielmetter, E.; Bronner-Fraser, M. N-Cadherin, a Cell Adhesion Molecule Involved in Establishment of Embryonic Left-Right Asymmetry. *Science* **2000**, *288*, 1047−1051.

(28) Gombotz, W. R.; Guanghui, W.; Horbett, T. A.; Hoffman, A. S. Protein Adsorption to Poly(Ethylene Oxide) Surfaces. *J. Biomed. Mater. Res.* **1991**, *25*, 1547−1562.

(29) Kratzer, D.; Ludwig-Husemann, A.; Junges, K.; Geckle, U.; Lee-Thedieck, C. Nanostructured Bifunctional Hydrogels as Potential Instructing Platform for Hematopoietic Stem Cell Differentiation. *Front. Mater.* **2019**, *5*, 00081.

(30) Guasch, J.; Conings, B.; Neubauer, S.; Rechenmacher, F.; Ende, K.; Rolli, C. G.; Kappel, C.; Schaufler, V.; Micoulet, A.; Kessler, H.; Boyen, H.-G.; Cavalcanti-Adam, E. A.; Spatz, J. P. Segregation Versus Colocalization: Orthogonally Functionalized Binary Micropatterned Substrates Regulate the Molecular Distribution in Focal Adhesions. *Adv. Mater.* **2015**, *27*, 3737−3747.

(31) Guasch, J.; Diemer, J.; Riahinezhad, H.; Neubauer, S.; Kessler, H.; Spatz, J. P. Synthesis of Binary Nanopatterns on Hydrogels for Initiating Cellular Responses. *Chem. Mater.* **2016**, *28*, 1806−1815.

(32) Guasch, J.; Hoffmann, M.; Diemer, J.; Riahinezhad, H.; Neubauer, S.; Kessler, H.; Spatz, J. P. Combining Adhesive Nanostructured Surfaces and Costimulatory Signals to Increase T Cell Activation. *Nano Lett.* **2018**, *18*, 5899−5904.

(33) Bilem, I.; Chevallier, P.; Plawinski, L.; Sone, E. D.; Durrieu, M.-C.; Laroche, G. Interplay of Geometric Cues and RGD/BMP-2 Crosstalk in Directing Stem Cell Fate. *ACS Biomater. Sci. Eng.* **2017**, *3*, 2514−2523.

https://dx.doi.org/10.1021/acsami.9b20939
ACS Appl. Mater. Interfaces 2020, 12, 22399−22409

(34) Biggs, M. J. P.; Richards, R. G.; McFarlane, S.; Wilkinson, C. D. W.; Oreffo, R. O. C.; Dalby, M. J. Adhesion Formation of Primary Human Osteoblasts and the Functional Response of Mesenchymal Stem Cells to 330 Nm Deep Microgrooves. *J. R. Soc., Interface* **2008**, *5*, 1231−1242.
(35) Abercrombie, M.; Heaysman, J. E. Observations on the Social Behaviour of Cells in Tissue Culture. II. Monolayering of Fibroblasts. *Exp. Cell Res.* **1954**, *6*, 293−306.
(36) Mui, K. L.; Chen, C. S.; Assoian, R. K. The Mechanical Regulation of Integrin-Cadherin Crosstalk Organizes Cells, Signaling and Forces. *J. Cell Sci.* **2016**, *129*, 1093−1100.
(37) Burute, M.; Thery, M. Spatial Segregation between Cell−Cell and Cell−Matrix Adhesions. *Curr. Opin. Cell Biol.* **2012**, *24*, 628−636.
(38) Borghi, N.; Lowndes, M.; Maruthamuthu, V.; Gardel, M. L.; Nelson, W. J. Regulation of Cell Motile Behavior by Crosstalk between Cadherin- and Integrin-Mediated Adhesions. *Proc. Natl. Acad. Sci. U. S. A.* **2010**, *107*, 13324−13329.
(39) Plestant, C.; Strale, P.-O.; Seddiki, R.; Nguyen, E.; Ladoux, B.; Mege, R.-M. Adhesive Interactions of N-Cadherin Limit the Recruitment of Microtubules to Cell-Cell Contacts through Organization of Actomyosin. *J. Cell Sci.* **2014**, *127*, 1660−1671.
(40) Cosgrove, B. D.; Mui, K. L.; Driscoll, T. P.; Caliari, S. R.; Mehta, K. D.; Assoian, R. K.; Burdick, J. A.; Mauck, R. L. N-Cadherin Adhesive Interactions Modulate Matrix Mechanosensing and Fate Commitment of Mesenchymal Stem Cells. *Nat. Mater.* **2016**, *15*, 1297−1306.
(41) Le Saux, G.; Edri, A.; Keydar, Y.; Hadad, U.; Porgador, A.; Schvartzman, M. Spatial and Chemical Surface Guidance of NK Cell Cytotoxic Activity. *ACS Appl. Mater. Interfaces* **2018**, *10*, 11486−11494.
(42) Huang, I.-H.; Hsiao, C.-T.; Wu, J.-C.; Shen, R.-F.; Liu, C.-Y.; Wang, Y.-K.; Chen, Y.-C.; Huang, C.-M.; Chang, Z.-F.; Tang, M.-J.; Khoo, K.-H.; Kuo, J.-C. GEF-H1 Controls Focal Adhesion Signaling That Regulates Mesenchymal Stem Cell Lineage Commitment. *J. Cell Sci.* **2014**, *127*, 4186.
(43) Yu, Y.-L.; Chou, R.-H.; Chen, L.-T.; Shyu, W.-C.; Hsieh, S.-C.; Wu, C.-S.; Zeng, H.-J.; Yeh, S.-P.; Yang, D.-M.; Hung, S.-C.; Hung, M.-C. EZH2 Regulates Neuronal Differentiation of Mesenchymal Stem Cells through PIP5K1C-Dependent Calcium Signaling. *J. Biol. Chem.* **2011**, *286*, 9657−9667.
(44) Pittenger, M. F.; Mackay, A. M.; Beck, S. C.; Jaiswal, R. K.; Douglas, R.; Mosca, J. D.; Moorman, M. A.; Simonetti, D. W.; Craig, S.; Marshak, D. R. Multilineage Potential of Adult Human Mesenchymal Stem Cells. *Science* **1999**, *284*, 143−147.
(45) Kilian, K. A.; Bugarija, B.; Lahn, B. T.; Mrksich, M. Geometric Cues for Directing the Differentiation of Mesenchymal Stem Cells. *Proc. Natl. Acad. Sci. U. S. A.* **2010**, *107*, 4872−4877.
(46) McBeath, R.; Pirone, D. M.; Nelson, C. M.; Bhadriraju, K.; Chen, C. S. Cell Shape, Cytoskeletal Tension, and RhoA Regulate Stem Cell Lineage Commitment. *Dev. Cell* **2004**, *6*, 483−495.
(47) Oya, K.; Tanaka, Y.; Saito, H.; Kurashima, K.; Nogi, K.; Tsutsumi, H.; Tsutsumi, Y.; Doi, H.; Nomura, N.; Hanawa, T. Calcification by MC3T3-E1 Cells on RGD Peptide Immobilized on Titanium through Electrodeposited PEG. *Biomaterials* **2009**, *30*, 1281−1286.
(48) Le Saux, G.; Plawinski, L.; Parrot, C.; Nlate, S.; Servant, L.; Teichmann, M.; Buffeteau, T.; Durrieu, M.-C. Surface Bound VEGF Mimicking Peptide Maintains Endothelial Cell Proliferation in the Absence of Soluble VEGF in Vitro. *J. Biomed. Mater. Res., Part A* **2016**, *104*, 1425.
(49) Keydar, Y.; Le Saux, G.; Pandey, A.; Avishay, E.; Bar-Hanin, N.; Esti, T.; Bhingardive, V.; Hadad, U.; Porgador, A.; Schvartzman, M. Natural Killer Cells' Immune Response Requires a Minimal Nanoscale Distribution of Activating Antigens. *Nanoscale* **2018**, *10*, 14651−14659.
(50) Hsiao, C.-T.; Cheng, H.-W.; Huang, C.-M.; Li, H.-R.; Ou, M.-H.; Huang, J. R.; Khoo, K. H.; Yu, H. W.; Chen, Y.-Q.; Wang, Y.-K.; Chiou, A.; Kuo, J.-C. Fibronectin in Cell Adhesion and Migration via N-Glycosylation. *Oncotarget* **2017**, *8*, 70653−70668.
(51) Ejim, O. S.; Blunn, G. W.; Brown, R. A. Production of Artificial-Orientated Mats and Strands from Plasma Fibronectin: A Morphological Study. *Biomaterials* **1993**, *14*, 743−748.
(52) Humphries, J. D.; Wang, P.; Streuli, C.; Geiger, B.; Humphries, M. J.; Ballestrem, C. Vinculin Controls Focal Adhesion Formation by Direct Interactions with Talin and Actin. *J. Cell Biol.* **2007**, *179*, 1043−1057.
(53) Leerberg, J. M.; Yap, A. S. Vinculin, Cadherin Mechanotransduction and Homeostasis of Cell−Cell Junctions. *Protoplasma* **2013**, *250*, 817−829.
(54) Bertocchi, C.; Wang, Y.; Ravasio, A.; Hara, Y.; Wu, Y.; Sailov, T.; Baird, M. A.; Davidson, M. W.; Zaidel-Bar, R.; Toyama, Y.; Ladoux, B.; Mege, R. M.; Kanchanawong, P. Nanoscale Architecture of Cadherin-Based Cell Adhesions. *Nat. Cell Biol.* **2017**, *19*, 28−37.
(55) Wein, F.; Pietsch, L.; Saffrich, R.; Wuchter, P.; Walenda, T.; Bork, S.; Horn, P.; Diehlmann, A.; Eckstein, V.; Ho, A. D.; Wagner, W. N-Cadherin Is Expressed on Human Hematopoietic Progenitor Cells and Mediates Interaction with Human Mesenchymal Stromal Cells. *Stem Cell Res.* **2010**, *4*, 129−139.
(56) Xu, J.; Zhu, C.; Zhang, Y.; Jiang, N.; Li, S.; Su, Z.; Akaike, T.; Yang, J. HE-Cadherin-Fc Fusion Protein Coated Surface Enhances the Adhesion and Proliferation of Human Mesenchymal Stem Cells. *Colloids Surf., B* **2013**, *109*, 97−102.
(57) Veiseh, M.; Wickes, B. T.; Castner, D. G.; Zhang, M. Guided Cell Patterning on Gold−Silicon Dioxide Substrates by Surface Molecular Engineering. *Biomaterials* **2004**, *25*, 3315−3324.
(58) Le Guéhennec, L.; Soueidan, A.; Layrolle, P.; Amouriq, Y. Surface Treatments of Titanium Dental Implants for Rapid Osseointegration. *Dent. Mater.* **2007**, *23*, 844−854.
(59) Bettinger, C. J.; Langer, R.; Borenstein, J. T. Engineering Substrate Topography at the Micro- and Nanoscale to Control Cell Function. *Angew. Chem., Int. Ed.* **2009**, *48*, 5406−5415.
(60) Loesberg, W. A.; te Riet, J.; van Delft, F. C. M. J. M.; Schön, P.; Figdor, C. G.; Speller, S.; van Loon, J. J. W. A.; Walboomers, X. F.; Jansen, J. A. The Threshold at Which Substrate Nanogroove Dimensions May Influence Fibroblast Alignment and Adhesion. *Biomaterials* **2007**, *28*, 3944−3951.
(61) Ramirez-San Juan, G. R.; Oakes, P. W.; Gardel, M. L. Contact Guidance Requires Spatial Control of Leading-Edge Protrusion. *Mol. Biol. Cell* **2017**, *28*, 1043−1053.
(62) Kasten, A.; Naser, T.; Brüllhoff, K.; Fiedler, J.; Müller, P.; Möller, M.; Rychly, J.; Groll, J.; Brenner, R. E. Guidance of Mesenchymal Stem Cells on Fibronectin Structured Hydrogel Films. *PLoS One* **2014**, *9*, No. e109411.
(63) den Braber, E. T.; de Ruijter, J. E.; Ginsel, L. A.; von Recum, A. F.; Jansen, J. A. Orientation of ECM Protein Deposition, Fibroblast Cytoskeleton, and Attachment Complex Components on Silicone Microgrooved Surfaces. *J. Biomed. Mater. Res.* **1998**, *40*, 291−300.
(64) Kim, D.-H.; Wirtz, D. Focal Adhesion Size Uniquely Predicts Cell Migration. *FASEB J.* **2013**, *27*, 1351−1361.
(65) Gavard, J.; Lambert, M.; Grosheva, I.; Marthiens, V.; Irinopoulou, T.; Riou, J.-F.; Bershadsky, A.; Mège, R.-M. Lamellipodium Extension and Cadherin Adhesion: Two Cell Responses to Cadherin Activation Relying on Distinct Signalling Pathways. *J. Cell Sci.* **2004**, *117*, 257−270.
(66) Zhang, Y.; Mao, H.; Qian, M.; Hu, F.; Cao, L.; Xu, K.; Shuai, Q.; Gao, C.; Lang, R.; Akaike, T.; Yang, J. Surface Modification with E-Cadherin Fusion Protein for Mesenchymal Stem Cell Culture. *J. Mater. Chem. B* **2016**, *4*, 4267−4277.
(67) Cavalcanti-Adam, E. A.; Volberg, T.; Micoulet, A.; Kessler, H.; Geiger, B.; Spatz, J. P. Cell Spreading and Focal Adhesion Dynamics Are Regulated by Spacing of Integrin Ligands. *Biophys. J.* **2007**, *92*, 2964−2974.
(68) Di Russo, J.; Young, J. L.; Balakrishnan, A.; Benk, A. S.; Spatz, J. P. NTA-Co3+-His6 versus NTA-Ni2+-His6 Mediated E-Cadherin Surface Immobilization Enhances Cellular Traction. *Biomaterials* **2019**, *192*, 171−178.

https://dx.doi.org/10.1021/acsami.9b20939
ACS Appl. Mater. Interfaces 2020, 12, 22399−22409

(69) Ladoux, B.; Anon, E.; Lambert, M.; Rabodzey, A.; Hersen, P.; Buguin, A.; Silberzan, P.; Mège, R.-M. Strength Dependence of Cadherin-Mediated Adhesions. *Biophys. J.* **2010**, *98*, 534−542.
(70) Balaban, N. Q.; Schwarz, U. S.; Riveline, D.; Goichberg, P.; Tzur, G.; Sabanay, I.; Mahalu, D.; Safran, S.; Bershadsky, A.; Addadi, L.; Geiger, B. Force and Focal Adhesion Assembly: A Close Relationship Studied Using Elastic Micropatterned Substrates. *Nat. Cell Biol.* **2001**, *3*, 466−472.
(71) Ray, A.; Lee, O.; Win, Z.; Edwards, R. M.; Alford, P. W.; Kim, D. H.; Provenzano, P. P. Anisotropic Forces from Spatially Constrained Focal Adhesions Mediate Contact Guidance Directed Cell Migration. *Nat. Commun.* **2017**, *8*, 14923.
(72) Mygind, T.; Stiehler, M.; Baatrup, A.; Li, H.; Zou, X.; Flyvbjerg, A.; Kassem, M.; Bünger, C. Mesenchymal Stem Cell Ingrowth and Differentiation on Coralline Hydroxyapatite Scaffolds. *Biomaterials* **2007**, *28*, 1036−1047.
(73) Ross, S. E.; Hemati, N.; Longo, K. A.; Bennett, C. N.; Lucas, P. C.; Erickson, R. L.; MacDougald, O. A. Inhibition of Adipogenesis by Wnt Signaling. *Science* **2000**, *289*, 950−953.
(74) Wang, Y.; Volloch, V.; Pindrus, M. A.; Blasioli, D. J.; Chen, J.; Kaplan, D. L. Murine Osteoblasts Regulate Mesenchymal Stem Cells via WNT and Cadherin Pathways: Mechanism Depends on Cell-Cell Contact Mode. *J. Tissue Eng. Regen. Med.* **2007**, *1*, 39−50.
(75) Radwanska, A.; Grall, D.; Schaub, S.; Beghelli-de la Forest Divonne, S.; Ciais, D.; Rekima, S.; Rupp, T.; Sudaka, A.; Orend, G.; Van Obberghen-Schilling, E. Counterbalancing Anti-Adhesive Effects of Tenascin-C through Fibronectin Expression in Endothelial Cells. *Sci. Rep.* **2017**, *7*, 12762.

https://dx.doi.org/10.1021/acsami.9b20939
ACS Appl. Mater. Interfaces 2020, 12, 22399−22409